nature photonics

SUPPLEMENTARY INFORMATION

DOI: 10.1038/NPHOTON.2012.300

Entanglement-enhanced probing of a delicate material system (Supplementary Information)

Florian Wolfgramm,[1] Chiara Vitelli,[2] Federica A. Beduini,[1] Nicolas Godbout,[3] and Morgan W. Mitchell[1,4]

[1]*ICFO – Institut de Ciencies Fotoniques, Mediterranean Technology Park, 08860 Castelldefels (Barcelona), Spain*
[2]*Center of Life Nanoscience at La Sapienza, Istituto Italiano di Tecnologia, Viale Regina Elena 255, 00181 Rome, Italy*
[3]*COPL, Département de Génie Physique, École Polytechnique de Montréal, C.P. 6079, Succ. Centre-ville, Montréal (Québec) H3C 3A7, Canada*
[4]*ICREA – Institució Catalana de Recerca i Estudis Avançats, 08015 Barcelona, Spain*

A. Model of atomic vapor magneto-optical properties

The cell, with an internal path of 75 mm and containing purified ^{85}Rb with a small (0.5%) admixture of ^{87}Rb, no buffer gas, and no wall coatings that might preserve polarization, is modeled as a thermal equilibrium, Doppler-broadened vapor subject to Zeeman shifts in the intermediate regime. The atomic structure is calculated by diagonalization of the atomic Hamiltonians $H_{\rm At}^{(\rm iso)} = H_0^{(\rm iso)} + H_{\rm HFS}^{(\rm iso)} + H_{\rm Z}^{(\rm iso)}$, where $H_0^{(\rm iso)}$ is the energy structure of the isotope $^{\rm iso}$Rb including fine-structure contribution, $H_{\rm HFS}^{(\rm iso)} = g_{\rm HFS}\mathbf{J}\cdot\mathbf{I}$ is the hyperfine contribution, and $H_{\rm Z}^{(\rm iso)} = \mathbf{b}\cdot(g_J\mathbf{J} + g_I\mathbf{I})$ is the Zeeman contribution. All atomic parameters are taken from refs 1,2. The matrices $H_{\rm At}^{(\rm iso)}$ are numerically diagonalized to find field-dependent energy eigenstates, illustrated in Fig. 6, from which the complex linear optical polarizability is calculated, including radiative damping. The complex refractive index $n_\pm$ for $\sigma_\pm$ polarizations is computed including Doppler broadening and a temperature-dependent atom density given by the vapor pressure times the isotope fraction, and the transfer function for the cell is calculated from the integral of the index along the beam path, including the measured drop in field strength of 15% from the center to the faces of the cell. The transfer functions are shown in Fig. 7.

B. Fisher information

The sensitivity of the measurement is computed using the Fisher information (FI)[3]

$$\mathcal{I}(B) = \sum_i P_i(\partial_B \ln P_i)^2. \qquad (3)$$

Fig. 8 shows $\mathcal{I}/2$, the FI per photon for the experimental NOON state ρ shown in Fig. 3. In an experiment with $N_{\rm tot} \gg 1$ total photons, the resulting magnetic uncertainty is $\delta B = (N_{\rm tot}\mathcal{I}/2)^{-1/2}$. Also shown is the standard quantum limit (SQL) for this figure of merit, i.e., the best possible FI per photon with non-entangled states, found by numerical optimization over possible single-photon inputs and the POVM $\{\Pi_i\}$. The NOON state achieves 1.30±0.05 improvement over the SQL, at a field $B = 37$ mT. All uncertainties given are one sigma statistical error. As with non-entangled photons (shown also in Fig. 8), the point of maximum sensitivity can be selected by varying the input polarization or by applying a bias magnetic field.

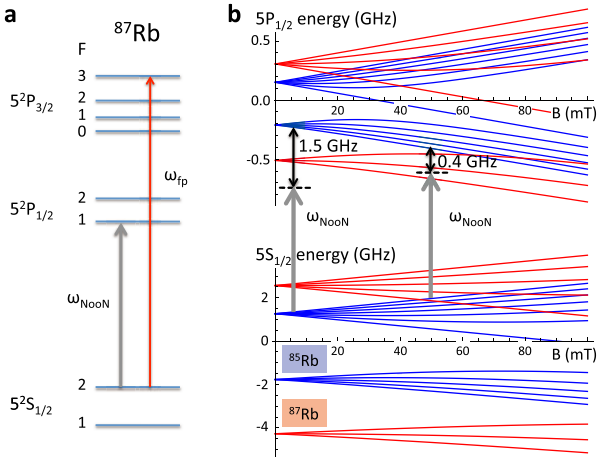

FIG. 6: Relevant energy level diagrams. **a** Energy levels of ^{87}Rb relevant to generation and filtering (not to scale). The frequency of the NOON state $\omega_{\rm NOON}$ is tuned to the $5^2{\rm S}_{1/2}{\rm F}{=}2 \rightarrow 5^2{\rm P}_{1/2}{\rm F}'{=}1$ transition of the D_1 line of ^{87}Rb. The optical pumping laser of the filter, with frequency $\omega_{\rm fp}$, addresses the $5^2{\rm S}_{1/2}{\rm F}{=}2 \rightarrow 5^2{\rm P}_{3/2}{\rm F}'{=}3$ transition of the D_2 line of ^{87}Rb. The 15 nm separation from the detection wavelength allows a high extinction using interference filters centered on $\omega_{\rm NOON}$. **b** D_1 energy levels of the probed ensemble versus field strength B, showing ^{85}Rb levels in blue and ^{87}Rb levels in red. At zero field $\omega_{\rm NOON}$ is 1.5 GHz detuned from the nearest ^{85}Rb transition. With increasing B, the nearest ^{85}Rb transition moves closer to resonance, increasing the Faraday rotation. The Doppler-broadened absorption begins to overlap $\omega_{\rm NOON}$ near $B = 50$ mT.

C. Fisher information per damage

The NOON state also gives an advantage in FI per scattered photon, the figure of merit for low-damage probing. We quantify scattering from the ^{85}Rb ensemble as $\mathcal{S} = {\rm Tr}[\rho\Pi_{\rm scat}]$, where $\Pi_{\rm scat} \equiv {\rm diag}(s_{++}, s_{+-}, s_{-+}, s_{--})$ in the $\sigma_\pm$ basis and the mean number of scattering events is $s_{ab} \equiv 2 - |t_a^{(85)}|^2 - |t_b^{(85)}|^2$, where $t_\pm^{(85)}$ is the ^{85}Rb contribution to $t_\pm$. A completely analogous calculation is made for single-photon scattering. As above, the the SQL for this figure of merit is found by numerical optimization. As shown in Fig. 4, the NOON state gives an advantage $(\mathcal{I}/\mathcal{S})_{\rm NOON}\,/(\mathcal{I}/\mathcal{S})_{\rm SQL} = 1.40\pm 0.06$ over the SQL.

DOI: 10.1038/NPHOTON.2012.300

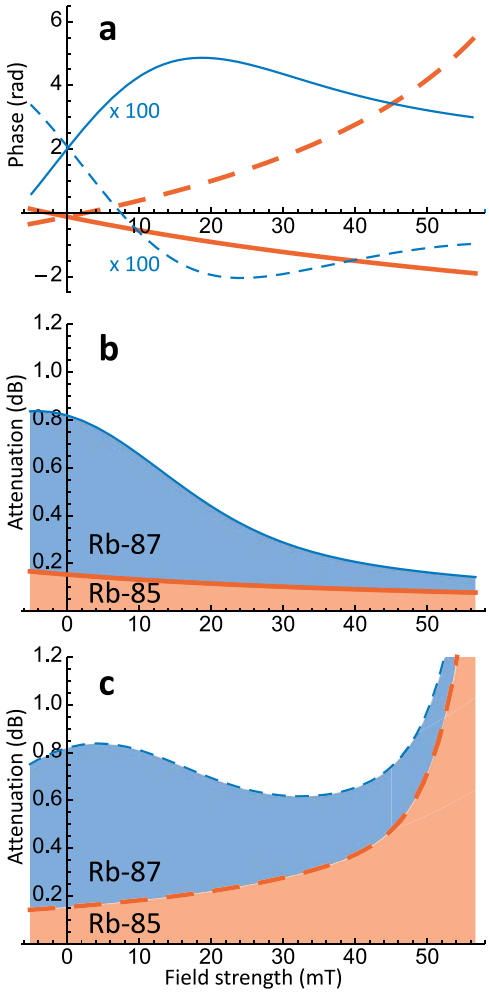

FIG. 7: Magneto-optical properties of the atomic ensemble, for probe light at ω_{NOON} , computed from model. Polarizations are shown by solid (σ_+) and dashed (σ_-) curves. Isotopic contributions are shown by thick orange (^{85}Rb) and thin blue (^{87}Rb) lines. **a** Phase retardation vs. field strength. The differential $\sigma_\pm$ retardation produces optical rotation. Contribution of ^{85}Rb is two orders of magnitude larger than that of ^{87}Rb, as expected from the isotopic ratio, and in the opposite sense. **b, c** Attenuation vs. field strength for σ_+, σ_- polarizations.

D. State reconstruction and statistical error of Fisher information

The state ρ is found by quantum state tomography from the data shown in Fig. 2, that is, by numerical search for the ρ that minimises the chi-squared distance between the predictions of equation (1) and the observed data. The optimized state is reported as the reconstructed ρ. To find statistical errors for the Fisher information, we search in the vicinity of ρ for states ρ' which maximize or minimize the Fisher information with a chi-squared distance at most δ larger than the optimum chi-squared. This establishes a statistical error which accounts for the non-linearity of the reconstruction procedure. The error ranges reported throughout are for $\delta = 1$, corresponding to $\pm 1\sigma$ in the case of a simple linear reconstruction.

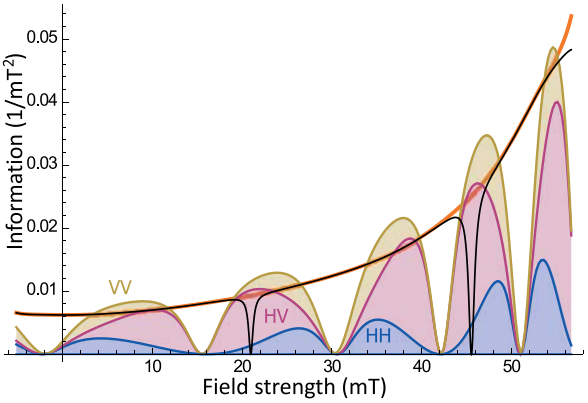

FIG. 8: Fisher information (FI) per input photon in Faraday rotation probing of the ensemble. Thin black curve shows FI for non-entangled photons of an arbitrarily chosen linear input polarization. Thick orange curve shows the "standard quantum limit," the largest FI obtainable with non-entangled states. Solid regions indicate contributions of HH, HV, and VV outcomes to the NOON state FI, calculated using ρ from Fig. 3. In all cases FI grows with increasing field, due to increased proximity to the ^{85}Rb resonances.

E. Relation to state-of-the-art detection

Thomas-Peter *et al.*[4] consider the effect of detector inefficiency and derive visibility thresholds for metrological advantage in scenarios with constant loss. These thresholds are not directly applicable to our scenario with polarization-dependent, parameter-dependent losses. We note that intrinsic losses are included already in the FI calculation, and because they are field-dependent, provide some information about B, offsetting the loss of FI due to non-arrival of pairs. Constant extrinsic losses including detector inefficiency reduce the NOON FI by η_{ex}^2 versus η_{ex} for any single-photon state. Current technology can achieve extrinsic efficiency of $\eta_{\mathrm{ex}} = \eta_{\mathrm{det}}\eta_{\mathrm{path}}$, with detector efficiency[5] $\eta_{\mathrm{det}} = 0.95$ and source-to-detector path efficiency[6] (including escape from the source cavity) $\eta_{\mathrm{path}} = 0.984$. With current technology, the NOON state demonstrated here gives a quantum enhancement of 1.21 ± 0.05 per sent photon and 1.15 ± 0.04 per photon scattered from the ^{85}Rb ensemble (1.31 ± 0.06 if the ^{87}Rb contaminant is removed).

F. Advantage for larger N NOON states

It is interesting to ask what advantage larger NOON states could give in this application. Considering ensemble transmissions t_L, t_R as above, and an in-

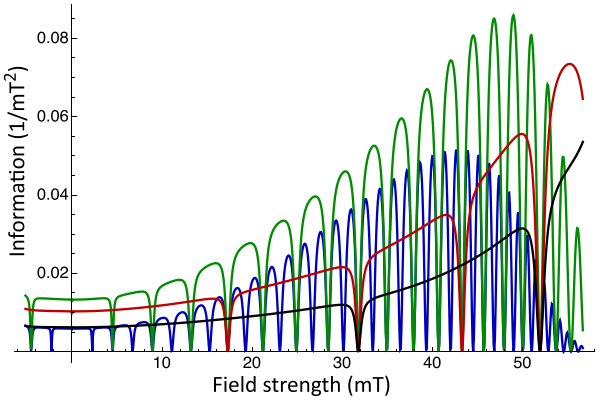

FIG. 9: Fisher information per input photon for ideal NOON states with $N = 1$ (black), 2 (red), 8 (green) and 16 (blue). For any given B, the trade-off between rotational sensitivity, which favours large N, and robustness, which favours small N, is optimized for finite N.

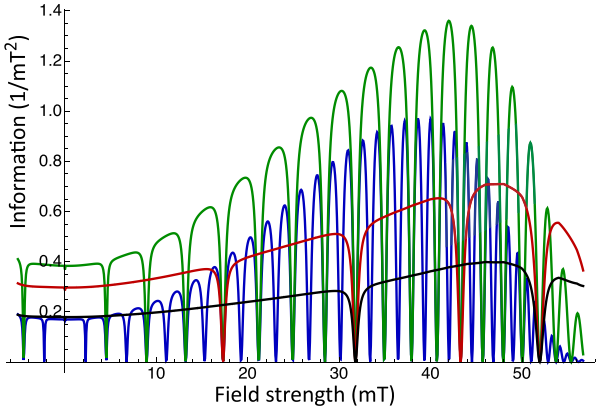

FIG. 10: Fisher information per scattered photon for NOON states with $N = 1$ (black), 2 (red), 8 (green), and 16 (blue).

put NOON state $|\mathrm{in}\rangle \equiv \frac{1}{\sqrt{2N!}}\left[(\mathrm{a}_\mathrm{L}^\dagger)^\mathrm{N} + (\mathrm{a}_\mathrm{R}^\dagger)^\mathrm{N}\right]|0\rangle$, we have an N-photon component of the output $|\mathrm{out}\rangle = \frac{1}{\sqrt{2N!}}\left[\mathrm{t}_\mathrm{L}^\mathrm{N}(\mathrm{a}_\mathrm{L}^\dagger)^\mathrm{N} + \mathrm{t}_\mathrm{R}^\mathrm{N}(\mathrm{a}_\mathrm{R}^\dagger)^\mathrm{N}\right]|0\rangle$. The detection, by projection onto states of the form $|N_H, N_V\rangle \equiv \frac{1}{\sqrt{N_H!N_V!}}(a_H^\dagger)^{N_H}(a_V^\dagger)^{N_V}|0\rangle$, gives N_V even or odd with probability $P_\mathrm{even} = |t_L^N + t_R^N|^2/4$, $P_\mathrm{odd} = |t_L^N - t_R^N|/4$, respectively. We use equation (3) to obtain the Fisher information, shown in Figures 9 and 10. For any given B, and optimal N exists, due to the trade-off between super-resolution and robustness.

G. Damage in quantum memory systems

The theory of dispersive measurement of spin ensembles is well described in the literature[7–14]. We restate some key results for gaussian states before considering the situation for NOON states. Consider an ensemble of $N_\mathrm{at} \gg 1$ spins with collective spin $\mathbf{F}$, in an initial state with $\langle F_\mathrm{x}\rangle \approx |\mathbf{F}|$ and $\langle F_\mathrm{y}^2 + F_\mathrm{z}^2\rangle \sim N_\mathrm{at} \ll \langle F_\mathrm{x}^2\rangle$. The small components $F_\mathrm{y}, F_\mathrm{z}$ are quantum observables and in a quantum memory context used to store quantum information. A probe consisting of $N_\mathrm{phot} \gg 1$ linearly-polarized photons experiences paramagnetic Faraday rotation by an angle $\phi = \kappa F_\mathrm{z}$, where F_z is the on-axis component of $\mathbf{F}$ and κ is a coupling constant determined by the beam geometry and spectroscopic parameters such as detuning. The optical polarization angle has input noise (variance) $\mathrm{var}(\phi) = N_\mathrm{phot}^{-1}$, and thus measurement noise (referred to the measured variable) of $\mathrm{var}(F_\mathrm{z}) = \kappa^{-2}N_\mathrm{phot}^{-1}$. The measurement also produces a back-action on $\mathbf{F}$, rotating it by an angle $\theta = \kappa S_\mathrm{z}^{(\mathrm{in})}$ about the F_z axis. Typically $\phi, \theta \ll 1$, so that

$$F_\mathrm{y}^{(\mathrm{out})} \approx F_\mathrm{y}^{(\mathrm{in})} + \kappa S_\mathrm{z} F_\mathrm{x}^{(\mathrm{in})}. \qquad (4)$$

Here $S_\mathrm{z} = \frac{1}{2}(n_L - n_R)$ is half the photon number difference between left- and right-circular polarisations. A single, linearly-polarized photon has polarisation noise $\mathrm{var}(S_\mathrm{z}) = \frac{1}{4}$, so the collection of N_phot independent photons has $\mathrm{var}(S_\mathrm{z}) = \frac{1}{4}N_\mathrm{phot}$ and introduces an additional noise $\mathrm{var}(F_\mathrm{y}) = \frac{1}{4}\kappa^2 N_\mathrm{phot}$, into $F_\mathrm{y}^{(\mathrm{out})}$.

When the same total number of photons are used, not as individuals but instead grouped into N-photon NOON states, the N-fold advantage (in FI or in variance) gives measurement uncertainty $\mathrm{var}(F_\mathrm{z}) = \kappa^{-2}N_\mathrm{phot}^{-1}N^{-1}$. Because the NOON state has $\mathrm{var}(S_\mathrm{z}) = \frac{1}{4}N^2$, the total back-action is correspondingly larger, $\mathrm{var}(F_\mathrm{y}) = \frac{1}{4}\kappa^2 N_\mathrm{phot}N$. In this idealized scenario, in which only the coherent polarization rotation is present, the use of NOON states is exactly equivalent to using a factor of N more photons in a non-entangled measurement.

When we consider damage processes, however, the NOON state gives an advantage not available to any classical state. The same light-matter interaction which produces the useful coherent rotation also produces incoherent scattering, which both removes photons from the probe beam and randomizes the spins of individual atoms. The total number of scattering events is $N_\mathrm{scat} = N_\mathrm{phot}N_\mathrm{at}\sigma(\Delta)/A$, where A is the cross-sectional area of the ensemble and $\sigma(\Delta)$ is the scattering cross-section, a function of the detuning Δ. The per-atom scattering $\eta \equiv N_\mathrm{scat}/N_\mathrm{at}$ is thus proportional to the per-photon scattering $\varepsilon \equiv N_\mathrm{scat}/N_\mathrm{phot}$, which we measure in the experiment. While quantitative details of the scattering-damage relation depend on the initial spin state and the structure of the probed system[12,15], the general features are evident in a spin-$\frac{1}{2}$ model, analyzed in detail in reference 11. As described there, scattering effectively removes a fraction η of the N_at atoms and replaces them with the same number of spin-randomized atoms. This reduces any signal as $\langle\mathbf{F}\rangle \to (1-\eta)\langle\mathbf{F}\rangle$ while introducing two noise sources, one from the breaking of correlations within the ensemble, the other from the introduction of random spins. From reference 11, equation (13), we learn that for $\eta \ll 1$, the spin variance changes as

$$\mathrm{var}(F_\mathrm{z}^2) \to (1-\eta)^2\mathrm{var}(F_\mathrm{z}^2) + 2\frac{1}{4}\eta N_\mathrm{at}. \qquad (5)$$

DOI: 10.1038/NPHOTON.2012.300

This combination of signal loss and added noise constitutes the damage to the state, with a strength determined by $\eta \propto \varepsilon$. A reduction in the number of scattered photons thus implies a corresponding reduction in damage.

The scattering by the ensemble is quantified in three ways in the experiment. First, it is directly observable in the coincidence detection rates, albeit with limited statistics. Second, it is measured spectroscopically with a weak laser beam, as shown in Fig. 5. Third, it is calculated from first principles using known atomic parameters. In these calculations, the vapor pressures of the two isotopes and the efficiency of the field coils are found by fitting to the spectroscopic data. As shown in Figures 2 and 5, we find very good agreement between these three methods. We use the calculated scattering when computing Fisher information per damage, because the computation is more accurate in the highly transparent low-B regime.

[1] Steck, D. A. Rubidium 85 D line data. Available online at http://steck.us/alkalidata (Revision 2.1.5, 19 September 2012).

[2] Steck, D. A. Rubidium 87 D line data. Available online at http://steck.us/alkalidata (Revision 2.1.4, 23 December 2010).

[3] Braunstein, S. L. & Caves, C. M. Statistical distance and the geometry of quantum states. *Phys. Rev. Lett.* **72,** 3439–3443 (1994).

[4] Thomas-Peter, N. *et al.* Real-world quantum sensors: Evaluating resources for precision measurement. *Phys. Rev. Lett.* **107,** 113603 (2011).

[5] Lita, A. E., Miller, A. J. & Nam, S. W. Counting near-infrared single-photons with 95% efficiency. *Opt. Express* **16,** 3032–3040 (2008).

[6] Vahlbruch, H. *et al.* Observation of squeezed light with 10-dB quantum-noise reduction. *Phys. Rev. Lett.* **100,** 033602 (2008).

[7] Duan, L.-M., Cirac, J. I., Zoller, P. & Polzik, E. S. Quantum communication between atomic ensembles using coherent light. *Phys. Rev. Lett.* **85**, 5643–5646 (2000).

[8] Smith, G. A., Chaudhury, S. & Jessen, P. S. Faraday spectroscopy in an optical lattice: a continuous probe of atom dynamics. *J. Opt. B* **5**, 323–329 (2003).

[9] Hammerer, C., Mølmer, K., Polzik, E. S. & Cirac, J. I. Light-matter quantum interface. *Phys. Rev. A* **70**, 044304 (2004).

[10] Mølmer, K. & Madsen, L. B. Estimation of a classical parameter with gaussian probes: Magnetometry with collective atomic spins. *Phys. Rev. A* **70**, 052102 (2004).

[11] Madsen, L. B. & Mølmer, K. Spin squeezing and precision probing with light and samples of atoms in the gaussian description. *Phys. Rev. A* **70**, 052324 (2004).

[12] de Echaniz, S. R. *et al.* Conditions for spin squeezing in a cold Rb-87 ensemble. *J. Opt. B* **7**, S548-S552 (2005).

[13] Geremia, J. M., Stockton, J. K. & Mabuchi, H. Tensor polarizability and dispersive quantum measurement of multilevel atoms. *Phys. Rev. A* **73**, 042112 (2006).

[14] Koschorreck, M. & Mitchell, M. W. Unified description of inhomogeneities, dissipation and transport in quantum light-atom interfaces. *J. Phys. B* **42**, 195502 (2009).

[15] Vasilyev, D. V., Hammerer, K., Korolev, N. & Sørensen, A. S. Quantum noise for Faraday light-matter interfaces. *J. Phys. B* **45**, 124007 (2012).